Importance of Photoelectron Multiple Scattering in the Iron K-Edge X-ray Absorption Spectra of Spin-Crossover Complexes: Full Multiple Scattering Calculations for Several Iron(II) Trispyrazolylborate and Trispyrazolylmethane Complexes

V. Briois,*,† Ph. Sainctavit,†,‡ Gary J. Long,*,§ and Fernande Grandjean||

LURE, UMR CNRS 130, Université Paris−Sud, F-91898 Orsay Cedex, France, LMCP, UMR CNRS 7590, UPMC/UDD/IPGP, Universités Paris VI et VII, 4 place Jussieu, F-75252 Paris Cedex 05, France, Department of Chemistry, University of Missouri−Rolla, Rolla, Missouri 65409-0010, and Institut de Physique, B5, Université de Liège, B-4000 Sart-Tilman, Belgium

Received June 27, 2000

Full multiple scattering calculations of the iron K-edge X-ray absorption near-edge spectra of the iron(II) low-spin complexes, $Fe[HB(pz)_3]_2$ and $\{Fe[HC(pz)_3]_2\}(BF_4)_2$ and high-spin complexes $Fe[HB(3,5\text{-}(CH_3)_2pz)_3]_2$ and $\{Fe[HC(3,5\text{-}(CH_3)_2pz)_3]_2\}(BF_4)_2$, where pz is the pyrazole ring, have been carried out. Excellent agreement with the experimental spectra is achieved when a basic 33-atom cluster, corresponding to $FeB_2C_{18}N_{12}$, is used for $Fe[HB(pz)_3]_2$, when four fluorine atoms are added to form a 37-atom cluster for $\{Fe[HC(pz)_3]_2\}(BF_4)_2$, and when 12 methyl carbon atoms are added to form a 45-atom cluster for $Fe[HB(3,5\text{-}(CH_3)_2pz)_3]_2$ and $\{Fe[HC(3,5\text{-}(CH_3)_2pz)_3]_2\}(BF_4)_2$. The full multiple scattering calculations with an increasing number of near-neighbor shells around the absorbing iron(II) ion reveal constructive and destructive contributions of subsequent shells upon the X-ray absorption spectral profiles. These calculations (1) permit an unambiguous assignment of specific absorption lines to scattering by specific near-neighbor shells, (2) reveal that medium-range scattering processes contribute significantly to the absorption profiles, and (3) permit a correlation between the shift in energy of the absorption edge upon going from a high-spin to a low-spin complex and the change in the distance of the first coordination shell around the absorbing iron(II) ion. The results of full multiple scattering calculations place constraints on the use of Natoli's rule in making assignments of absorption lines to near-neighbor shells.

Introduction

For the past 10 years X-ray absorption spectroscopy has been commonly used to characterize the structural and electronic changes exhibited by many pseudooctahedral $3d^4$ to $3d^7$ transition metal complexes as they undergo a spin crossover or a spin transition.[1−19] This technique has several advantages over X-ray diffraction because it may be used for studying crystalline or amorphous solids, liquids, and solutions. Further, its elemental and angular momentum selectivity probes the final state of a specific atom or ion, in this paper iron(II). At the metal K-edge, excitations from the 1s core level to unoccupied *n*p levels are involved, whereas at the metal $L_{2,3}$-edges, excitations from the 2p core level to unoccupied 3d levels are involved.[8,17−19]

Many of the earlier papers[1−2,5−7,9−16] are devoted to metal K-edge extended X-ray absorption fine structure studies or EXAFS studies, and they report both the local arrangement around the metal atom or ion and the structural modifications associated with the spin crossover or the spin transition. In some papers the X-ray absorption near-edge structure spectra, the XANES spectra, have also been reported[1,4,6,8−11,13,15−16] at the metal K-edge.

† Université Paris−Sud.
‡ Universités Paris VI et VII.
§ University of Missouri−Rolla.
|| Université de Liège.

(1) Cartier, C.; Thuery, P.; Verdaguer, M.; Zarembowitch, J.; Michalowicz, A. *J. Phys.* **1986**, *C8*, 563.
(2) Thuéry, P.; Zarembowitch, J.; Michalowicz, A.; Kahn, O. *Inorg. Chem.* **1987**, *26*, 851.
(3) Briois, V.; Cartier, C.; Momenteau, M.; Maillard, P.; Zarembowitch, J.; Dartyge, E.; Fontaine, A.; Tourillon, G.; Thuery, P.; Verdaguer, M. *J. Chim. Phys.* **1989**, *86*, 1623.
(4) Roux, C.; Zarembowitch, J.; Itié, J.-P.; Verdaguer, M.; Dartyge, E.; Fontaine, A.; Tolentino, H. *Inorg. Chem.* **1991**, *30*, 3174.
(5) Michalowicz, A.; Moscovici, J.; Ducourant, B.; Cracco, D.; Kahn, O. *Chem. Mater.* **1995**, *7*, 1833.
(6) Chen, L. X.; Wang, Z.; Burdett, J. K.; Montano, P. A.; Norris, J. R. *J. Phys. Chem.* **1995**, *99*, 7958.
(7) Bausk, N. V.; Erenburg, S. B.; Lavrenova, L. G.; Mazalov, L. N. *J. Struct. Chem.* **1995**, *36*, 925.
(8) Briois, V.; Cartier dit Moulin, C.; Sainctavit, P.; Brouder, C.; Flank, A. M. *J. Am. Chem. Soc.* **1995**, *117*, 1019.
(9) Zamponi, S.; Gambini, G.; Conti, P.; Gioia Lobbia, G.; Marassi, R.; Berrettoni, M.; Cecchi, P. *Polyhedron* **1995**, *14*, 1929.
(10) Roux, C.; Zarembowitch, J.; Itié, J.-P.; Polian, A.; Verdaguer, M. *Inorg. Chem.* **1996**, *35*, 574.
(11) Roux, C.; Adams, D. M.; Itié, J.-P.; Polian, A.; Hendrikson, D. N.; Verdaguer, M. *Inorg. Chem.* **1996**, *35*, 2846.
(12) Erenburg, S. B.; Bausk, N. V.; Varnek, V. A.; Lavrenova, L. G. *J. Magn. Magn. Mater.* **1996**, *157−158*, 595.
(13) Young, N. A. *J. Chem. Soc., Dalton Trans.* **1996**, 1275.
(14) Sankar, G.; Thomas, J. M.; Varma, V.; Kulkarni, G. U.; Rao, C. N. R. *Chem. Phys. Lett.* **1996**, *251*, 79.
(15) Real, J. A.; Castro, I.; Bousseksou, A.; Verdaguer, M.; Burriel, R.; Castro, M.; Linares, J.; Varret, F. *Inorg. Chem.* **1997**, *36*, 455.
(16) Hannay, C.; Hubin-Franskin, M. J.; Grandjean, F.; Briois, V.; Itié, J. P.; Polian, A.; Trofimenko, S.; Long, G. J. *Inorg. Chem.* **1997**, *36*, 5580.
(17) Cartier dit Moulin, C.; Rudolf, P.; Flank, A. M.; Chen, C. T. *J. Phys. Chem.* **1992**, *96*, 6196.
(18) Abbate, M.; Fuggle, J. C.; Fujimori, A.; Tjeng, L. H.; Chen, C. T.; Potze, R.; Sawatzky, G.; Eisaki, H.; Uchida, S. *Phys. Rev. B* **1993**, *47*, 16124.
(19) Collison, D.; Garner, D.; McGrath, C. M.; Mosselmans, J. F. W.; Roper, M. D.; Seddon, J. M. W.; Sinn, E.; Young, N. A. *J. Chem. Soc., Dalton Trans.* **1997**, 4371.

10.1021/ic0007153 CCC: $20.00
Published on Web 01/27/2001

The changes in the XANES spectra observed at a spin crossover are often interpreted[3−4,10−11] on the basis of a rather simple molecular orbital approach based on metal and ligand atomic orbitals. An alternative approach to understanding these spectra involves a full multiple scattering calculation of the photoelectron scattering. This approach has been used to try to understand the changes observed[8] at the spin crossover in the iron K-edge XANES spectra of *cis*-Fe(phen)$_2$(NCS)$_2$, where phen is 1,10-phenanthroline. The changes in these spectra have been related completely to changes in the crystallographic structure, changes that result from the 3d electronic changes at the spin crossover. The structural changes give rise to differences in the photoelectron multiple scattering path lengths, differences that lead to changes in the relative intensities and energies of the absorption lines in high-spin and low-spin XANES spectra.

In general, the contribution of a specific backscattering shell, at a distance r from the absorbing metal atom or ion, is expected to contribute an XANES spectral absorption line whose energy is approximated by Natoli's rule, $Er^2 =$ constant, a rule that is based on multiple scattering theory.[20] Various authors[6,8,21−26] have used constants ranging from 150 to 300 eV Å^2 in order to assign specific XANES spectral features to specific interatomic distances in a molecule.

This paper has two goals: (1) to confirm the correlation between the XANES spectral absorption energies and the characteristic bond lengths found in a specific compound or set of related compounds and (2) to identify the absorption profile associated with a specific coordination shell in a compound. To achieve these goals, a cluster approach used in conjunction with a full multiple scattering calculation is essential. The first step in the calculation separates and identifies the absorption profile resulting from the first coordination shell, an identification that is essential in evaluating the validity and limitations of any molecular orbital interpretation of XANES spectral features.[1,4,6,9−11,13,15,16]

In previous papers we have reported[16,27,28] an iron K-edge X-ray absorption spectral study of several iron(II) and cobalt(II) pyrazolylborate and pyrazolylmethane complexes, some of which exhibit an electronic spin crossover. Herein, we report full multiple scattering calculations for these complexes for which the crystallographic structures have been reported.[27−29] These complexes include the low-spin complex Fe[HB(pz)$_3$]$_2$, **1**, and the high-spin complex Fe[HB(3,5-(CH$_3$)$_2$pz)$_3$]$_2$, **2**, where pz is the planar pyrazole ring (see Figure 1a). In addition, we report on the analogous methane complexes in which boron has been replaced by carbon to form the low-spin complex {Fe[HC(pz)$_3$]$_2$}(BF$_4$)$_2$, **3**, and the high-spin complex {Fe[HC(3,5-(CH$_3$)$_2$pz)$_3$]$_2$}(BF$_4$)$_2$, **4**. It should be noted that complexes **1** and **3** remain low-spin upon cooling to 78 K, whereas complexes **2** and **4** undergo a spin crossover from the high-spin to the low-spin state upon cooling to 78 K.

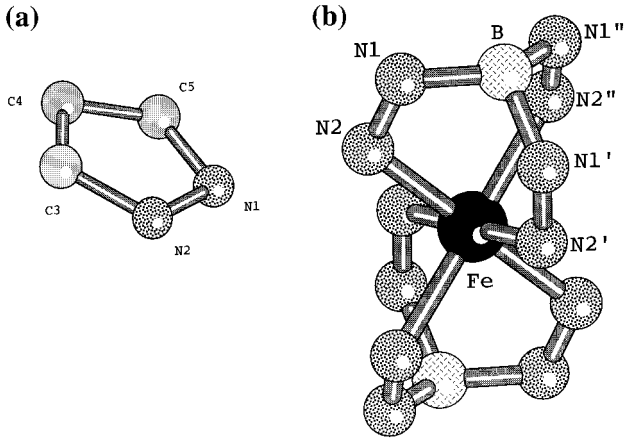

Figure 1. Pyrazolyl moiety (a) and the iron near-neighbor environment (b) in Fe[HB(pz)$_3$]$_2$, **1**, and Fe[HB(3,5-(CH$_3$)$_2$pz)$_3$]$_2$, **2**. In {Fe[HC(pz)$_3$]$_2$}(BF$_4$)$_2$, **3**, and {Fe[HC(3,5-(CH$_3$)$_2$pz)$_3$]$_2$}(BF$_4$)$_2$, **4**, carbon replaces boron. For clarity the carbon atoms C3, C4, and C5 of the pyrazole rings are omitted from part b.

Both the hydrotris(1-pyrazolyl)borate and hydrotris(3,5-dimethyl-1-pyrazolyl)borate anions, as well as the analogous neutral methane ligands, act as tridentate ligands, forming distorted octahedral iron(II) complexes (see Figure 1b). In all of the complexes studied herein the iron(II) ions have the same coordination environment with the same first and second shell near-neighbors (see Table 1). However, as indicated in Table 1, small distance differences do exist beyond 3 Å for the subsequent shells in the different compounds. Furthermore, in complexes **3** and **4** additional backscattering from the fluorine of the two BF$_4$ anions is possible.

The origin of the changes in the XANES spectra observed at the spin crossover may be easily understood because the structural changes occurring upon the high-spin to low-spin crossover in **2** and **4** are dominated by a decrease in the iron(II) first coordination shell distance with no associated rearrangement of the ligands. Furthermore, a comparison between the experimental and calculated XANES spectra of **1**−**4** should reveal whether the near-edge spectral features are sensitive to medium and/or short-range contributions to the scattering.

Full Multiple Scattering Calculations

The X-ray absorption cross-section for the transition from the initial state, |i⟩, to the final state, |f⟩, is given by

$$\sigma(\hbar\omega) = 4\pi^2\alpha\hbar\omega\sum_{\mathrm{f}}|\langle \mathrm{f}|\bar{\epsilon}\cdot\bar{r}|i\rangle|^2\,\delta(E_{\mathrm{f}}-E_{\mathrm{i}}-\hbar\omega)$$

where $\bar{\epsilon}.\bar{r}$ is the electric dipole transition operator, α is the fine structure constant, E_{i} and E_{f} are the initial and final energies of states i and f, and δ is the Dirac function. The full multiple scattering formalism is a method for solving the one-electron Schrödinger equation, a formalism that permits the calculation of the initial and final state wave functions from a "muffin-tin" potential of a finite cluster of atoms about an absorbing atom or ion.

Full multiple scattering calculations have been performed by using the extended CONTINUUM code developed by Natoli and coworkers.[30,31] The X-ray absorption cross sections have been calculated

(20) Natoli, C. R. Near Edge Structure III. *Springer Proc. Phys.* **1984**, *2*, 38.
(21) Lytle, F. W. *Ber. Bunsen-Ges. Phys. Chem.* **1987**, *91*, 1251.
(22) Lytle, F. W.; Gregor, R. B.; Panson, A. J. *Phys. Rev. B* **1988**, *37*, 1550.
(23) Mahto, P.; Chetal, A. R. *Physica B* **1989**, *58*, 415.
(24) Sinha, R. N.; Mahto, P.; Chetal, A. R. *Z. Phys. B: Condens. Matter* **1990**, *81*, 229.
(25) Kasrai, M.; Fleet, M. E.; Bancroft, G. M.; Tan, K. H.; Chen, J. M. *Phys. Rev. B* **1991**, *43*, 1763.
(26) Chen, J. M.; Simons, J. K.; Tan, K. H.; Rosenberg, R. A. *Phys. Rev. B* **1993**, *48*, 10047.
(27) Reger, D. L.; Little, C. A.; Rheingold, A. L.; Lam, M.; Concolino, T.; Mohan, A.; Long, G. J. *Inorg. Chem.* **2000**, *39*, 4674.
(28) Reger, D. L.; Little, C. A.; Rheingold, A. L.; Lam, M.; Concolino, T.; Mohan, A.; Long, G. J.; Briois, V.; Grandjean, F. *Inorg. Chem.*, in press.
(29) Oliver, J. D.; Mullica, D. F.; Hutchinson, B. B.; Milligan, W. O. *Inorg. Chem.* **1980**, *19*, 165.
(30) Kutzler, F. W.; Natoli, C. R.; Misemer, D. K.; Doniach, S.; Hodgson, K. O. *J. Chem. Phys.* **1980**, *73*, 3274.
(31) Natoli, C. R.; Misemer, D. K.; Doniach, S.; Kutzler, F. W. *Phys. Rev. A* **1980**, *22*, 1104.

Table 1. Composition of the Various Atom Clusters Used in the Full Multiple Scattering Calculations

Fe[HB(pz)$_3$]$_2$, **1**				{Fe[HC(pz)$_3$]$_2$}(BF$_4$)$_2$, **3**				Fe[HB(3,5-(CH$_3$)$_2$(pz)$_3$]$_2$, **2**				{Fe[HC(3,5-(CH$_3$)$_2$(pz)$_3$]$_2$}(BF$_4$)$_2$, **4**			
size	atom	no.	distance, Å	size	atom	no.	distance, Å	size	atom	no.	distance, Å	size	atom	no.	distance, Å
7	N2	6	1.98	7	N2	6	1.97	7	N2	6	2.17	7	N2	6	2.17
13	N1	6	2.90	13	N1	6	2.88	13	N1	6	3.05	13	N1	6	3.04
19	C3	6	3.06	15	C	2	3.01	15	B	2	3.18	15	C	2	3.14
21	B	2	3.08	21	C3	6	3.08	21	C3	6	3.28	21	C3	6	3.28
27	C5	6	4.08	27	C5	6	4.10	27	C5	6	4.26	27	C5	6	4.27
33	C4	6	4.19	33	C4	6	4.21	33	C4	6	4.40	33	C4	6	4.39
				37	F	4	4.76	39	C[a]	6	3.73	39	C[a]	6	3.75
								45	C[b]	6	5.54	45	C[b]	6	5.53
												47	F	2	5.59
												49	F	2	5.78

[a] The carbon atom of the methyl group at the 3 position of the pyrazol ring. [b] The carbon atom of the methyl group at the 5 position of the pyrazol ring.

at the iron K-edge for the low-spin complexes **1** and **3** and for the high-spin complexes **2** and **4** to reproduce the XANES spectra. The calculations for the four complexes are based on various, differently sized clusters centered on the absorbing iron(II) ion derived from earlier single-crystal X-ray structural studies.[28,29] These calculations used exactly the same structures, and hence bond distances, as those reported earlier, and no attempt was made to change the bond distances during these calculations. Thus, the errors associated with the distances given in Table 1 are the same as those derived from the X-ray structural work and are typically ±0.002 to ±0.003 Å for the iron to near-neighbor nitrogen bond distances.

The basic cluster used for all four complexes is the 33-atom Fe[B(C$_3$N$_2$)$_3$]$_2$ or Fe[C(C$_3$N$_2$)$_3$]$_2$ moiety (see Table 1). In addition, the influence of the methyl substitution at the 3 and 5 positions of the pyrazolyl rings has been investigated for complexes **2** and **4** by using a cluster of 45 atoms. Finally, the closer fluorine atoms have been added for complexes **3** and **4**, yielding clusters with 37 and 49 atoms, respectively. No hydrogen atoms have been included in any of the scattering calculations because of the well-known weak scattering power of hydrogen.

The muffin-tin potentials within which the photoelectron scattering occurs are constructed as described by Levelut et al.[32] The atomic charge densities have been generated by using the Clementi and Roetti self-consistent field atomic functions.[33] The muffin-tin radii have been obtained according to the Norman criterium[34] and have been used without overlap. The muffin-tin potential has been obtained through a superposition of neutral charge densities to which has been added an exchange and correlation potential obtained either with the *X*-α formulation with the Schwartz[35] coefficients or with the complex Hedin−Lundqvist formulation.[36,37] The photoelectron effective mean free path, λ_{eff}, in the final state is calculated from the imaginary part of the Hedin−Lundqvist potential. To take into account the core−hole lifetime, a constant damping factor, Γ, of 1.9 eV has been added to the imaginary part of the photoelectron self-energy. When the spectra are calculated with the complex Hedin−Lundqvist potential, the computed features are smooth because of the damping of the excited photoelectron by intrinsic and extrinsic inelastic losses.

The charge relaxation around the core hole in the absorbing atom has been simulated by using the so-called "relaxed and screened" approximation.[32] To take into account the relaxation, the excited-state orbitals with the iron 1s core hole are considered to be similar to the ground-state orbitals of the $Z + 1$ atom, i.e., the cobalt atom. To take into account the screening, the core electron is promoted to a 3d valence orbital.

(32) Levelut, C.; Sainctavit, P.; Ramos, A.; Petiau, J. *J. Phys.: Condens. Matter* **1995**, *7*, 2353.
(33) Clementi, E.; Roetti, C. *At. Data Nucl. Data Tables* **1974**, *14*, 177.
(34) Norman, D. *Phys. Rev. Lett.* **1983**, *51*, 2052.
(35) Schwartz, K. *Phys. Rev. B* **1972**, *5*, 2466.
(36) Hedin, L.; Lundqvist, B. I. *J. Phys. C* **1971**, *4*, 2064.
(37) Gunella, R.; Benfatto, M.; Marcelli, A.; Natoli, C. R. *Solid State Commun.* **1980**, *76*, 109.

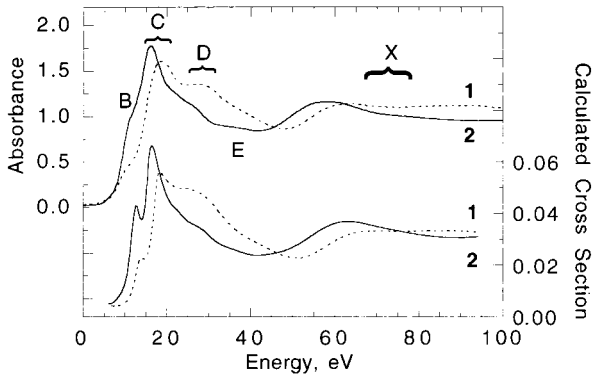

Figure 2. Observed 295 K iron K-edge XANES spectra and the calculated spectra for low-spin Fe[HB(pz)$_3$]$_2$, **1** (dotted line), and for high-spin Fe[HB(3,5-(CH$_3$)$_2$pz)$_3$]$_2$, **2** (solid line). Clusters of 33 and 45 atoms have been used in the full multiple scattering calculations for complexes **1** and **2**, respectively.

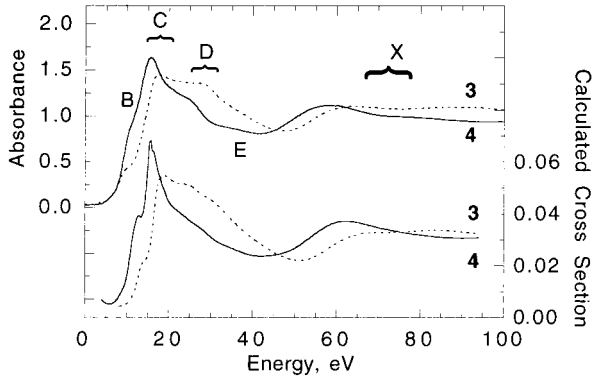

Figure 3. Observed 295 K iron K-edge XANES spectra and the calculated spectra for low-spin {Fe[HC(pz)$_3$]$_2$}(BF$_4$)$_2$, **3** (dotted line), and for high-spin {Fe[HC(3,5-(CH$_3$)$_2$pz)$_3$]$_2$}(BF$_4$)$_2$, **4** (solid line). Clusters of 37 and 45 atoms have been used in the full multiple scattering calculations for complexes **3** and **4**, respectively.

Results

Excellent agreement between the calculated and observed XANES spectra has been obtained, as shown in Figure 2 for complexes **1** and **2** and in Figure 3 for complexes **3** and **4**. The experimental spectra obtained for complexes **1**−**4** are the same as the spectra reported earlier.[16,28] More specifically the experimental spectra of Fe[HB(pz)$_3$]$_2$, **1**, shown in Figure 2, is the same as the 295 K spectra shown in Figure 1 of ref 16, and the experimental spectrum of Fe[HB(3,5-(CH$_3$)$_2$pz)$_3$]$_2$, **2**, shown in Figure 2 is the 77 K spectrum reported but not shown in ref 16. The experimental spectra of {Fe[HC(pz)$_3$]$_2$}(BF$_4$)$_2$, **3**, and

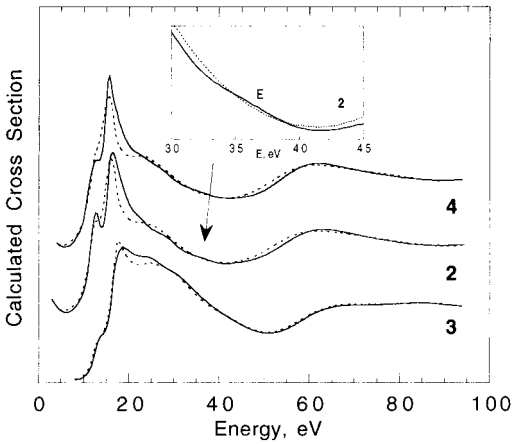

Figure 4. Calculated XANES spectra for different clusters in complexes **2**−**4**. The dashed lines refer to the 33-atom clusters for complexes **2**−**4**, and the solid lines refer to the 45-, 37-, and 49-atom clusters for complexes **2**, **3**, and **4**, respectively. The inset shows the detailed differences between 3.0 and 4.5 eV in the calculated spectrum of **2** for 33- and 45-atom clusters.

$\{Fe[HC(3,5\text{-}(CH_3)_2pz)_3]_2\}(BF_4)_2$, **4**, shown in Figure 3 are the same as the 295 K spectra shown in Figure 11 of ref 28. The calculated spectra have been obtained for clusters of 33 atoms for complex **1**, 45 atoms for complex **2**, 37 atoms for complex **3**, and 45 atoms for cluster **4**. These calculations have used the complex Hedin−Lundqvist potential. The zero in energy of the experimental spectra corresponds to the first maximum in the derivative of the iron foil K-edge spectrum[16] at 7112 eV. To compare the experimental and theoretical XANES spectra, the main calculated absorption line, labeled C in Figures 2 and 3 for the high-spin complexes **2** and **4**, is aligned with the corresponding experimental absorption line.

Full multiple scattering calculations with the complex Hedin−Lundqvist potential are shown in Figure 4 for the smallest and largest clusters as defined in Table 1 for complexes **2**−**4**. For complex **4** the calculation with the 49-atom cluster, i.e., with fluorine atoms, is virtually identical to the 45-atom cluster calculated spectrum shown in Figure 3.

Full multiple scattering calculations for complexes **1** and **2** with increasing cluster size (see Table 1) are shown in Figure 5. In this figure, to make the different calculated absorption lines sharper, the calculations have been carried out with the *X*-α formulation for the exchange potential without any consideration of broadening due to the core hole, instrumental resolution, or inelastic losses. In these calculations there is no bandwidth parameter, and the changes in the broadness of the absorption lines in Figure 5 result only from changes in the number of electronic transitions involved in the resonance. For a given complex, the same value of the mean interstitial *X*-α exchange potential has been used for the different clusters, values that correspond to that found for the 33- and 45-atom cluster for complexes **1** and **2**, respectively. As a consequence, all the calculations have a common reference energy.

Discussion

As shown in Figures 2 and 3, both the general shape of the experimental spectra and the relative variation in the intensity and energy of the absorption lines for the high-spin and low-spin complexes are satisfactorily reproduced by our full multiple scattering calculations. The procedure for aligning the experimental and calculated spectra of the high-spin complexes **2** and **4** has been given above. This procedure also implies the analogous alignment of the experimental and calculated spectra

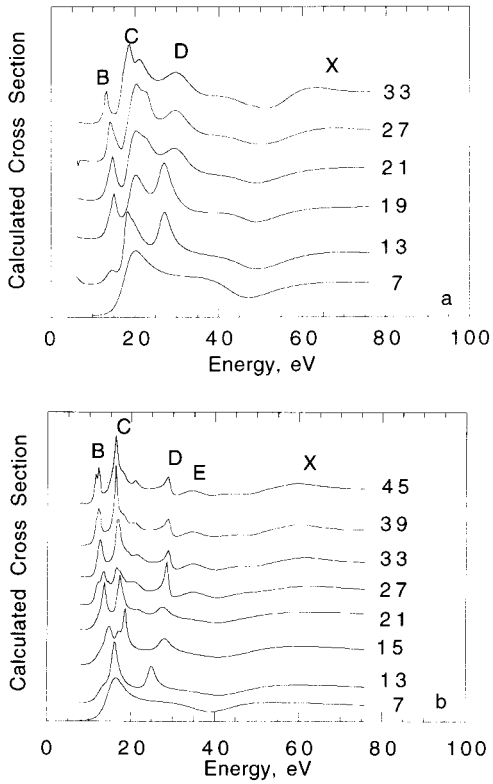

Figure 5. XANES spectra calculated with the indicated number of cluster atoms for $Fe[HB(pz)_3]_2$, **1** (a), and $Fe[HB(3,5\text{-}(CH_3)_2pz)_3]_2$, **2** (b).

of the low-spin complexes **1** and **3**, an alignment that is excellent. Thus, the experimental shift in energy of absorption lines C, D, and X for the low-spin complexes, compared to those of the high-spin complexes, is directly related to the shorter multiple scattering pathways in the low-spin complexes (see Table 1).

Because the electronic spin state plays no part in the construction of the scattering potential, the differences in the potentials for the low-spin and high-spin complexes result only from the changes in the molecular structures, changes that lead to differences in the multiple scattering pathways. The calculation of the scattering potential does not take into account the difference in occupancy of the t_{2g} and e_g iron 3d orbitals for the different spin states. Rather, the calculations have been carried out for both the low-spin and high-spin iron complexes by starting from the same Clementi and Roetti atomic wave functions.[33] Thus, the differences between the high- and low-spin simulations arise mainly from differences in the structures of the complexes and not from initial differences in the electronic occupancy of the iron t_{2g} and e_g orbitals. Similar results have been obtained for $Fe(phen)_2(NCS)_2$ above and below its spin-crossover temperature.[8] The work reported herein and the earlier work on $Fe(phen)_2(NCS)_2$ clearly establish the structural origin of the XANES spectral absorption lines at the iron K-edge and show that the multiple scattering framework is a suitable theory for mimicking the hybridization between the 4s and 4p states of iron and the symmetry-adopted atomic orbitals of the neighboring atoms.

As is observed in Figures 2 and 3, full multiple scattering calculations are successful in reproducing even small relative changes in intensity of spectral absorption lines. Specifically, the difference in intensity between both the experimental and calculated spectral absorption lines C and D in complex **3** (see

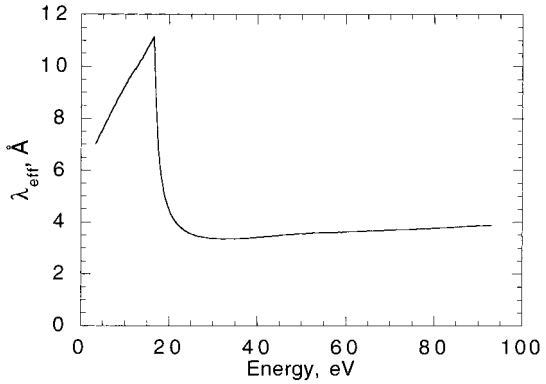

Figure 6. Energy dependence of the effective mean free path of the photoelectron at the iron K-edge.

Figure 3) is smaller than the equivalent difference for complex **1** (see Figure 2).

The introduction of the methyl groups, which substitute for hydrogen at the 3 and 5 positions of the pyrazolyl ring, into the calculations performed on the high-spin complexes (see Figure 4) clearly improves the agreement between experimental and calculated spectra. Specifically, the small plateau labeled E at ca. 35 eV in Figures 2 and 3 is better reproduced with the 45-atom cluster, a cluster that includes the 12 carbon atoms of the methyl groups (see Table 1). Thus, *even* the methyl groups are involved in the multiple scattering processes. Our previous study[16] of the iron(II) and cobalt(II) pyrazolylborate complexes had already revealed this experimentally because the cobalt K-edge spectrum of high-spin $Co[HB(pz)_3]_2$ does not show the absorption plateau at E whereas the spectrum of high-spin $Co[HB(3,5\text{-}(CH_3)_2pz)_3]_2$ does. Although the addition of methyl induces the spin crossover, the contribution of the methyl group carbon to the multiple scattering is small and could not be confirmed[16] without the use of full multiple scattering calculations.

The addition of four of the eight fluorines belonging to the two BF_4 anions also improves the agreement between the observed and calculated spectra, especially for low-spin complex **3**. Specifically, absorption lines C and D are better reproduced by the 37-atom, fluoride-containing cluster than by the 33-atom cluster (see Figure 4). This result clearly indicates that the features in the spectral energy range below ca. 30 eV are strongly dominated by medium-range scattering and thus requires clusters of ca. 5 Å radius to be accurately reproduced. Because fluorine is heavier than nitrogen and carbon, its scattering power is strong enough to substantially change the shape of absorption lines C and D.

Our full multiple scattering calculations for complexes **1** and **2** as a function of scattering cluster size (see Figure 5) lead to several important conclusions. First, the inclusion of successive shells leads to the detailed structure observed in the XANES spectra. Second, the shape of the XANES spectra results from scattering processes involving several different shells. Constructive and/or destructive superposition effects occur, to varying degrees, as subsequent shells are added to the multiple scattering calculation. The occurrence of these "interference-like" phenomena produces drastic changes in the number and intensity of the spectral absorption lines. The need to include all of these shells in the calculation indicates that all these shells are located at distances shorter than the average mean free path of the photoelectron, an effective mean free path that is obtained from the imaginary part of the Hedin−Lundqvist potential (see Figure 6). This figure shows that the mean free path in the energy range above ca. 20 eV is between 3 and 4 Å and, as a consequence, the XANES spectral lines are dominated by shells located at distances of less than 4 Å. The calculated spectra shown in Figure 5 indicate that for both complexes the two furthest shells (see Table 1) lead, both above and below 20 eV, to only minor changes in the shape of the XANES spectra. These changes are normally hidden by the broadening of the absorption bands due to extrinsic and intrinsic losses. The same argument can be used to explain the negligible influence of the four fluorine atoms in the 49-atom cluster on the XANES spectrum of compound **4** (see Figures 3b and 4). Indeed, these fluorine atoms are found at ca. 5.7 Å from the iron(II) ion, a distance that is larger than the photoelectron effective mean free path of ca. 5 Å.

By considering the calculations performed for the different shells, it appears that some of the absorption bands can be related to a specific shell. First, absorption line X, which is reproduced with a seven-atom cluster, is mainly determined by scattering processes inside the first coordination shell. As noted earlier,[16] the energy of X for complexes **1** and **2** verifies the Natoli rule,[20] and hence, absorption line X may be unambiguously assigned to scattering within the first coordination shell of nitrogen atoms. Second, as shown in Figure 5 for complexes **1** and **2**, absorption line D is present at the proper energy for all calculations with clusters larger than 21 and 15 atoms, respectively. In both **1** and **2**, absorption D corresponds to the introduction of two boron atoms into the cluster, but because of changes in the crystallographic structures, boron is found in different shells (see Table 1), and as a consequence, the assignment of absorption D is unambiguous. As a consequence of the limited mean free path of the photoelectron (see above and Figure 6), the energy of absorption line D is not affected by the addition of more distant shells.

Full multiple scattering calculations performed with the 33-atom cluster and with the same cluster without the two boron atoms are shown in Figure 7. It appears that the energy of *only* absorption line D is significantly affected by the addition of the boron. Furthermore, a comparison of the calculated XANES spectra for complexes **1** and **3** indicates that only the energy of absorption line D changes when boron is replaced by carbon. This occurs because the two boron atoms in complex **1** form the fourth shell at 3.08 Å whereas the two carbon atoms in complex **3** form the third shell at 3.01 Å (see Table 1). Hence, in agreement with Natoli's rule, the energy of absorption line D is lower in complex **1** than in complex **3**. Consequently, the results presented in Figures 5 and 7 permit the unambiguous assignment of absorption line D to scattering by shells containing either boron or the methane carbon.

Finally, the intensity and number of calculated spectral absorption lines between 10 and 20 eV vary considerably with cluster size. The more intense absorptions for the 13-atom cluster of the two complexes are located at the energy of absorption line C in Figure 5. Considering clusters with a higher number of atoms, we observe a "splitting" of the more intense absorptions to yield lines B and C. In the calculation corresponding to the largest clusters, absorption line C is found at the expected experimental energy. The fact that absorption line C is already located at the correct energy in the 13-atom cluster does not permit a direct assignment to the second nitrogen shell. Nevertheless, the cluster with 13 atoms constructively contributes to this spectral absorption.

A full multiple scattering calculation of the contributions of the different shells of atoms in a given molecule reveals, unambiguously, the origin of the different absorptions lines in

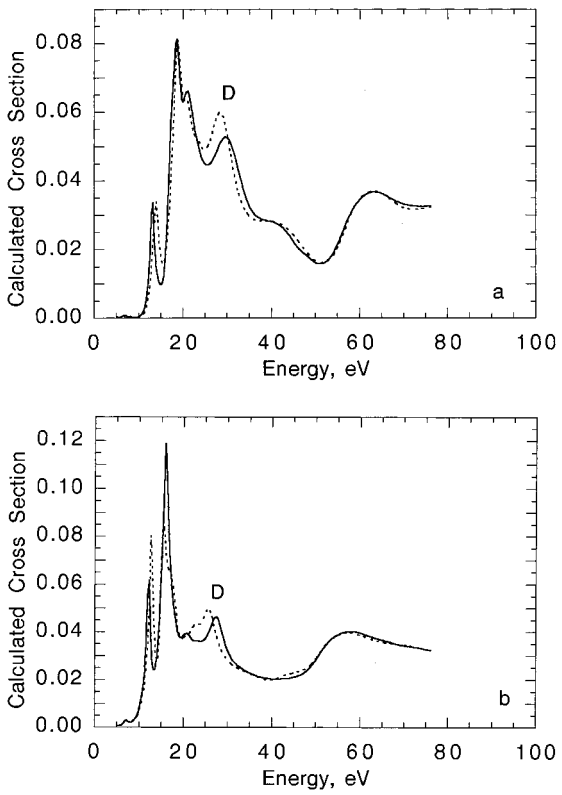

Figure 7. Comparison of the calculated XANES spectra for a 31-atom cluster (dotted line) and for a 33-atom cluster (solid line) in Fe[HB(pz)$_3$]$_2$, **1** (a), and Fe[HB(3,5-(CH$_3$)$_2$pz)$_3$]$_2$, **2** (b). The atom clusters are the same except the two boron atoms have been removed in the 31-atom cluster.

an XANES spectrum. Despite the evident complexity of the scattering processes that give rise to the XANES spectral lines, several authors[6,8,21−26] have attempted to correlate a given shell with a given absorption. Specifically, the XANES spectra of the pseudooctahedral Fe(α-picolamine)$_3$]Cl$_2$·EtOH complex[6,38,39] obtained above and below the spin-crossover temperature have a shape very similar to those observed herein for the low-spin and high-spin complexes. These XANES spectra have been interpreted[6] with Natoli's rule[20] as reformulated by Lytle.[22] Unfortunately, this earlier work[6] assumed that single scattering processes were dominant over the 10−40 eV energy range, a conclusion that is in conflict with the work reported herein (see below).

On the basis of the work of Chen et al.,[6] we would have to assign absorption line D to scattering by the first nitrogen shell and absorption line C to scattering by the second shell of neighbors located at ca. 3.05 Å for high-spin complexes **2** and **4** and at ca. 2.90 Å for low-spin complexes **1** and **3**. Once again, on the basis of our full multiple scattering calculations, these assignments would clearly be incorrect. As mentioned above, the second shell of neighbors constructively contributes to

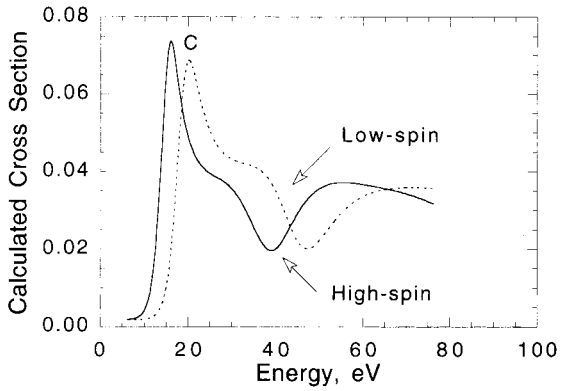

Figure 8. Calculated XANES spectra for a seven-atom cluster at an iron(II) ion in a low-spin and a high-spin complex.

absorption line C, but this feature clearly originates from scattering by several shells. Furthermore, the seven-atom cluster calculation shown in Figure 5 indicates that the first nitrogen coordination shell constructively contributes to absorption line D through the presence of a large shoulder at ca. 30−35 eV.

The seven-atom cluster calculated spectra shown in Figure 5 are typical of the XANES spectra of pure octahedral complexes, such as the first-row transition metal ion hexaaquo complexes.[40] Previously we have shown[40] that for octahedral ML$_6$ complexes multiple scattering pathways, such as the M → L → M → L′ → M pathway, where L and L′ are centrosymmetrically located ligands, contribute significantly to absorption line D. Hence, the dominant scattering effect is a triple scattering processes and not single scattering as proposed by Chen et al.[6] In addition, our calculations show that the presence of two boron or carbon atoms in more distant shells gives rise to added details in the shoulder present in the seven-atom cluster calculation. Without the support of full multiple scattering calculations, it is not possible to eliminate similar effects in the [Fe(α-picolamine)$_3$]Cl$_2$·EtOH complex.

The seven-atom cluster calculations shown in Figure 8 reproduce the observed shift in experimental energy and the variation in intensity in going from a low-spin to a high-spin complex. Hence, the distances to the first coordination shell of 1.98 Å in the low-spin complexes and of 2.17 Å in the high-spin complexes play a major role in the energy position of the rising absorption edge. This conclusion is important because the commonly used[3,4,10,11] molecular orbital interpretation of the XANES spectra explains qualitatively the energy shift and intensity change of the XANES absorption C in going from the low-spin to the high-spin state. In this molecular orbital approach, the shift in energy of the rising edge is understood in terms of the different electronic configurations of the high-spin and low-spin states. In the low-spin state, all six of the iron 3d electrons are in nonbonding or weakly π-antibonding t_{2g} orbitals, whereas in the high-spin state two of these electrons are promoted to the σ-antibonding e_g orbitals. This promotion is associated with an increase in bond length in the high-spin complexes, an increase that reduces the σ-antibonding overlap between the 4p orbitals of iron(II) and the predominantly 2p nitrogen orbitals. Consequently, the σ-antibonding state, with a strong 4p character, is stabilized relative to its energy in the low-spin complexes, and as a consequence, the rising edge shifts to lower energy. The increase in intensity of absorption line C (see Figure 8) is also a consequence of the reduction of the

(38) Mikami, M.; Konno, M.; Saito, Y. *Acta Crystallogr. B* **1980**, *36*, 275.
(39) In [Fe(α-picolamine)$_3$]Cl$_2$·EtOH the α-picolamine ring acts as a bidendate ligand, with both nitrogen atoms of each picolamine ring coordinated to iron(II), to yield a pseudooctahedral dicationic complex (see ref 38). The 290 K high-spin XANES spectrum of [Fe(α-picolamine)$_3$]Cl$_2$·EtOH has a maximum absorption at ca. 16.5 eV, a maximum that is shifted to ca. 20.5 eV in the 10 K low-spin spectrum (see Figure 2 of ref 6). This shift is accompanied by a simultaneous reduction in the relative intensity of the line, and further, a shoulder at ca. 30 eV increases in intensity upon cooling from 290 to 10 K. These features directly correspond to the absorption lines C and D of complexes **1** and **2** (see Figure 2).
(40) Briois, V.; Lagarde, P.; Brouder, C.; Sainctavit, P.; Verdaguer, M. *Physica B* **1995**, *208−209*, 52.

overlap between the lowest unoccupied 4p iron(II) orbital and the highest occupied 2p nitrogen orbital, a reduction that gives rise to an increase in the density of the iron(II) empty states. The results of the full multiple scattering calculations for the seven-atom cluster are in line with the molecular orbital approach to understanding the changes in the XANES spectra occurring at a spin crossover.

Conclusions

This study has shown that any interpretation of XANES spectra based solely on single scattering processes and Natoli's rule may be questionable. In contrast, full multiple scattering calculations permit an assignment of the different absorption lines to different near-neighbor shells about an absorbing atom. This study has also demonstrated the additive[41] "building block" character of the multiple scattering contributions to an XANES spectrum. A comparison of complexes **1** and **2** with complexes **3** and **4** has indicated that many details in the XANES spectra originate in medium-range scattering processes. Specifically, the full multiple scattering calculations show that distant anions, such as the BF_4 anion, must be considered in the scattering processes in order to accurately reproduce an XANES spectrum. Full multiple scattering calculations with increasing cluster size also permit an assignment of some XANES absorption lines to a given near-neighbor shell; the energy of these lines corresponds to that predicted by Natoli's rule. However, because of the building block character of the XANES spectra, it is dangerous, solely on the basis of Natoli's rule, to make an assignment of a given absorption to a specific near-neighbor shell. Finally, full multiple scattering calculations have shown that the shift in energy of the absorption edge of the XANES spectrum, upon going from a high-spin to a low-spin complex, is a consequence of the change in the distance of the first coordination shell.

Acknowledgment. The authors acknowledge, with thanks, the support obtained from the European Commission for Human Capital and Mobility, Contract ERBCHXCT930360. This research was also supported in part by the U.S. National Science Foundation through Grant DMR95-21739.

IC0007153

(41) Kizler, P. *Phys. Rev. B* **1992**, *46*, 10540.